Thermochimica Acta, 226 (1993) 187–200
Elsevier Science Publishers B.V., Amsterdam

Application of isothermal calorimetry and UV spectroscopy for stability monitoring of pentaerythritol tetranitrate [1]

Larry R. Dosser and James M. Pickard *
EG&G Mound [2] Applied Technologies, Miamisburg, OH 45343-0987 (USA)
(Received 26 October 1992; accepted 20 April 1993)

Abstract

Thermal stabilities for three pentaerythritol tetranitrate (PETN) samples with variable surface areas were monitored by isothermal calorimetry and UV spectroscopy over the range 363–408 K. Isothermal induction times measured with constant volume calorimetry under an air atmosphere, and NO evolution rates monitored by UV absorbance at 213 nm under vacuum correlated with the PETN surface area at temperatures equal or exceeding 383 K. Rate data measured at 383 K are in accord with predictions based on detailed kinetic modeling. Below 383 K, NO evolution data suggested that additional geometric factors may be significant in controlling PETN stability. Mechanisms for the influence of surface area upon the rate-determining step are addressed.

INTRODUCTION

Advancing applications technology coupled with increased enivornmental, safety, and health regulations require accurate and precise methods for surveying the stability of energetic materials subjected to long-term aging. These requirements necessitate the need for a more fundamental understanding of the chemistry, in particular the kinetics for degradation, of pentaerythritol tetranitrate (PETN). In previous work, it was demonstrated that an atmosphere of NO_2 above PETN within a closed system reduced the isothermal induction time, as recorded by conventional isothermal calorimetry [1]. These results were shown to be quantitatively in accord with a simple phenomenological model based on an autocatalytic rate law arising

* Corresponding author.
[1] Presented at the 21st Annual NATAS Conference, Atlanta, GA, 13–16 September 1992.
[2] Mound is operated by EG&G Mound Applied Technologies for the U.S. Department of Energy under Contract No. DE-AC04-88DP43495.

from combined melt–decomposition and secondary chain initiation by NO_2. In this paper, the influence of surface area upon the low-temperature aging of PETN and evolution of NO was investigated by isothermal calorimetry and UV spectroscopy. Rate data are shown to be in accord with detailed kinetic modeling for the decomposition of PETN. Specific mechanisms to account for the influence of surface area upon the low-temperature degradation of PETN and the evolution of NO and NO_2 are discussed.

EXPERIMENTAL

Samples of PETN with surface areas of 5000, 5500, and 12 000 $cm^2\,g^{-1}$ were prepared by proprietary processing methods. The specified surface areas possessed an uncertainty of ±10%. Isothermal induction times for PETN were recorded with a Setaram C-80 calorimeter over the range 393–408 K. For a typical run, 20 mg samples of PETN were sealed in 0.15 cm^3 stainless steel crucibles under an air atmosphere. For an induction time measurement, the sealed crucible was placed in the center of the C-80 detector and data were collected until completion of the exotherm. Induction time was defined as the time-to-maximum rate (TMR).

Evolution of NO was recorded with a Shimadzu UV-260 spectrophotometer at 213 nm. UV spectroscopy was conducted in conjunction with C.J. Seliskar, Center for Laser Chemistry, University of Cincinnati, Cincinnati, OH. Samples were prepared by loading 100 mg of PETN into a small pyrex vessel to which a 5 cm × 1 cm^2 suprasil quartz optical cell (cuvette) was attached via a graded seal. The cell had a total volume of approximately 6 cm^3, and was attached to a greaseless glass manifold with black wax via an 18/9 ball joint. The cell was then evacuated to a pressure of 2×10^{-5} torr with a turmolecular pump and sealed. Prior to this final sealing, however, the region of the vessel where the seal was to be made was flamed with a glassblower's torch while pumping on the vessel. The powder was not exposed to elevated temperature during this procedure, and was continually pumped to prevent any decomposition products from adhering to the power. The pressure was monitored with an ion gauge to follow the off-gasing from the thermal decomposition of PETN in the vessel seal-off region. When significant amounts of gas were evolved, the heating was discontinued and the vessel was reevacuated to a pressure of 2×10^{-5} torr. This process was repeated until no significant pressure increase was observed with additional flaming of the seal-off region. At this point the portion of the vessel containing the sample was cooled under liquid N_2, and the vessels were evacuated and sealed at 2×10^{-5} torr. The samples were subjected to isothermal aging in a convection oven for 260 days. Periodically, the vessels were removed from the oven and NO pressure was determined from the absorption band at 213 nm.

KINETIC MODELING

A semi-implicit Euler method [2] employing a step size of 10^{-7} was used to solve the initial value problem for decomposition of PETN under vacuum at 383 K. Product evolution profiles were determined by solution of a series of stiff differential equations expressed in the general form

$$\frac{d[R_i]}{dt} = \sum_j k_{ij}[R_j][RH] - \left[\sum_j k_j[RH]\right][R_i] + \text{Initiation} + \text{Termination} \quad (1)$$

where R_i and R_j are intermediate radicals, RH is any molecular species, k_{ij} is the specific rate constant for production of R_i from R_j and RH, and k_j is the specific rate constant for destruction of R_i by reaction with RH. A complete list of all reactions and rate constants used in the model is given in Appendices A and B. The sensitivity of the calculated NO evolution profile with respect to the rate constants was assessed by varying the activation energies for selected reactions.

The model was based on the following heterogeneous initiation mechanism:

(1, −1)	$C(CH_2ONO_2)_4(c)$	$\rightleftharpoons C(CH_2ONO_2)_4$
(2, −2)	$C(CH_2ONO_3)_4(c)$	$\rightleftharpoons C(CH_2ONO_2)_3CH_2O + NO_2$
(3, −3)	$C(CH_2ONO_2)_4$	$\rightleftharpoons C(CH_2ONO_2)_3CH_2O + NO_2$
(4)	$C(CH_2ONO_2)_3CH_2O$	$\rightarrow C(CH_2ONO_2)_3 + H_2CO$
(5)	$C(CH_2ONO_2)_3$	$\rightarrow 2CH_3ONO_2 + 2CO + NO$
(6)	$C(CH_2ONO_2)_3$	$\rightarrow 2CH_2ONO_2 + NO + H_2CO + CO$
(7, −7)	CH_3ONO_2	$\rightleftharpoons CH_3O + NO_2$

where $C(CH_2ONO_2)_4(c)$ corresponds to PETN in the crystalline phase. All other species are assumed to be in the gas phase. Reactions (2), (4), and (5) were proposed by Ng et al. [3] on the assumption of solid state kinetics. Reaction (6) was postulated in the present work as an alternative pathway for destruction of the trimethylene nitrate methyl radical $C(CH_2ONO_2)_3$, formed in reaction (4). Secondary propagation and transfer reactions listed in Appendix A which lead to the observed product distribution for PETN (primarily CO, CO_2, H_2O, N_2O, NO_2, NO, N_2, H_2CO) arise from gas phase decomposition of CH_3ONO_2.

Values for the specific rate constants were taken from the literature [3–10] and selected compilations [11–13]. Rate constants for reactions (5) and (6) were estimated from group additivity with the assumption of "half-bonded" five-center transition states [14]. Termination reactions, i.e.

recombination of atoms or small polyatomic radicals, were expressed as $k_c[R_i][R_j][M]$ where k_c is the recombination rate constant and M is a third body. The pressure of M was assigned a reasonable value of 150 torr.

RESULTS

Representative thermograms for the decomposition of PETN at 398 K with three different surface areas are illustrated in Fig. 1. A summary of the TMR data for each PETN sample is given in Table 1. In order to quantify the temperature dependence of TMR, the apparent reaction rate was expressed as

$$\frac{d\alpha}{dt} = A10^{-E/\theta} f(\alpha) \tag{2}$$

where $d\alpha/dt$ is the dimensionless rate, A is the apparent pre-exponential factor, E is the activation energy, $f(\alpha)$ is a function related to the reaction mechanism, and θ is $2.303RT$ kJ mol^{-1}. Rearrangement of eqn. (2) and integration from 0 to the time-to-maximum rate yields

$$\log[\mathrm{TMR}^{-1}] = \log A\left[\int f(\alpha_m)^{-1}\, d\alpha\right]^{-1} - \frac{E}{\theta} \tag{3}$$

where α_m is the extent of reaction at the TMR. Equation (3) indicates that a plot of $\log[\mathrm{TMR}^{-1}]$ versus the reciprocal of the absolute temperature should yield a straight line with a slope of $E/(2.303R)$ and an intercept of $\log A[\int f(\alpha_m)^{-1}\, d\alpha]^{-1}$. A rate plot based on eqn. (3) for average values of the TMR data is given in Fig. 2.

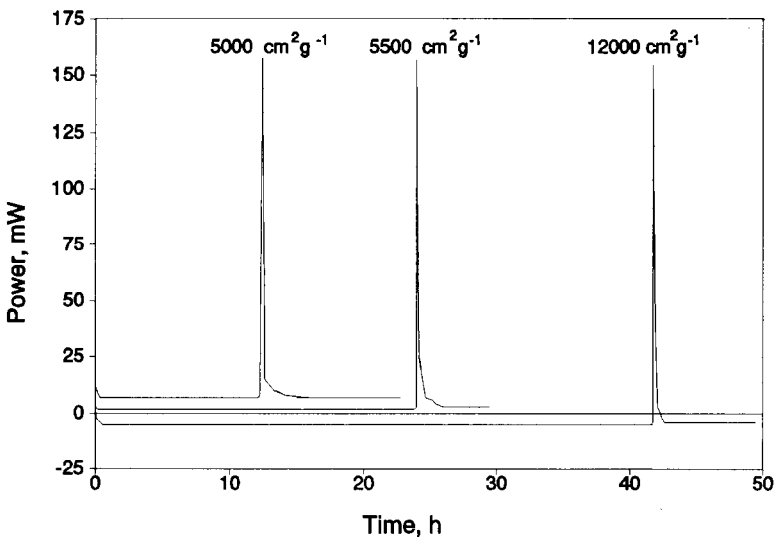

Fig. 1. Influence of surface area on TMR for PETN decomposition at 398 K.

TABLE 1

Summary of TMR data for PETN decomposition

Surface area/$cm^2\ g^{-1}$	# Obs.	Temperature/K	TMR/h [a]
5000	4	408	3.1 ± 0.1
	8	403	8.6 ± 1.4
	6	398	13.6 ± 2.1
	6	393	23.0 ± 5.9
5500	4	408	3.7 ± 0.1
	6	403	11.1 ± 0.9
	5	398	28.2 ± 2.1
	5	393	48.3 ± 5.5
12 000	4	408	4.1 ± 0.3
	6	403	15.4 ± 1.1
	4	398	40.2 ± 4.2
	6	393	164.6 ± 41.0

[a] Error estimates are one standard deviation.

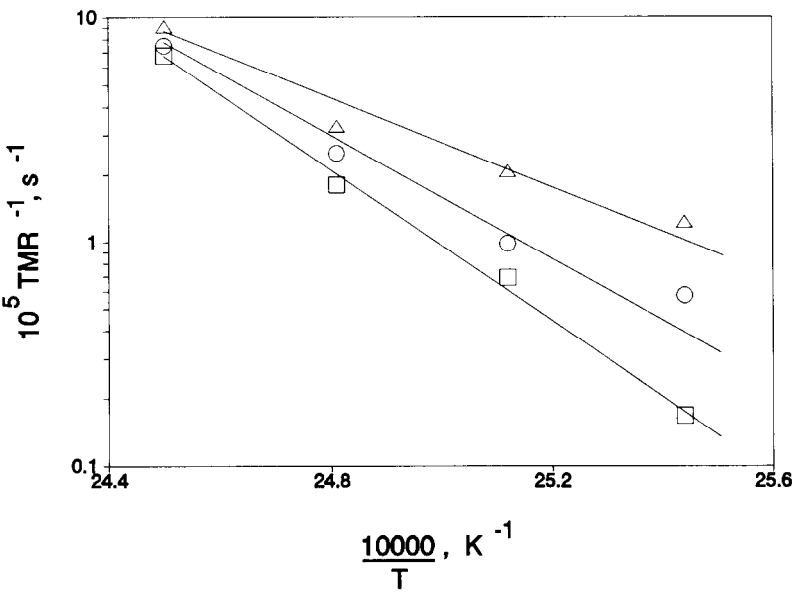

Fig. 2. Rate plot for PETN decomposition from 408 to 393 K: △, 5000 $cm^2\ g^{-1}$; ○, 5500 $cm^2\ g^{-1}$; □, 12 000 $cm^2\ g^{-1}$.

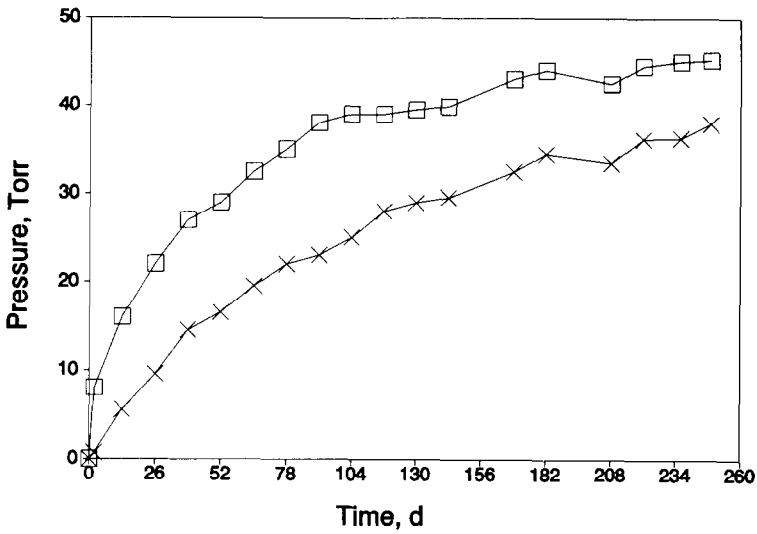

Fig. 3. Observed NO evolution from PETN at 383 K: □, 5000 $cm^2 g^{-1}$; ×, 5500 $cm^2 g^{-1}$.

Reaction profiles for evolution of NO determined at 383 and 363 K under vacuum by UV for PETN with initial surface areas in the range of 5000 to 12 000 $cm^2 g^{-1}$ are given in Figs. 3 and 4. Figure 5 is a comparison of the NO evolution for PETN with an initial surface area of 5500 $cm^2 g^{-1}$ to results obtained from kinetic modeling for PETN under vacuum at 383 K. Figure 6 illustrates the calculated NO evolution at 383 K for PETN under an initial pressure of 15 torr of NO_2.

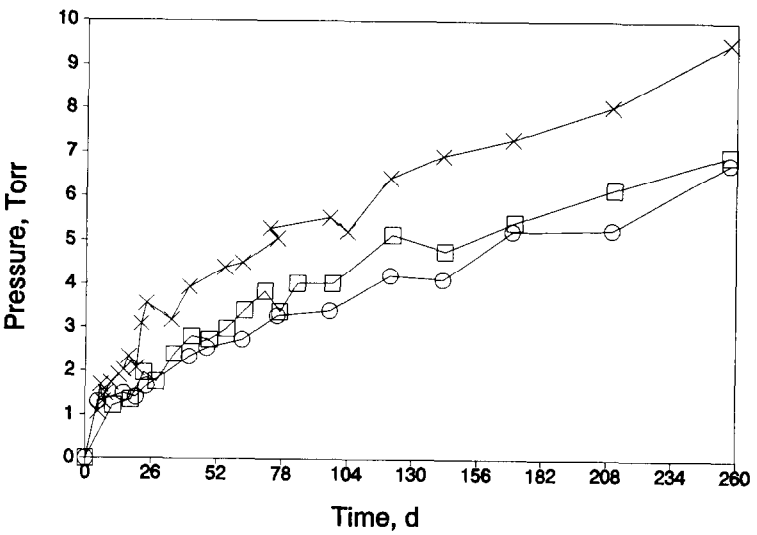

Fig. 4. Observed NO evolution from PETN at 363 K: □, 5000 $cm^2 g^{-1}$; ○, 5500 $cm^2 g^{-1}$; ×, 12 000 $cm^2 g^{-1}$.

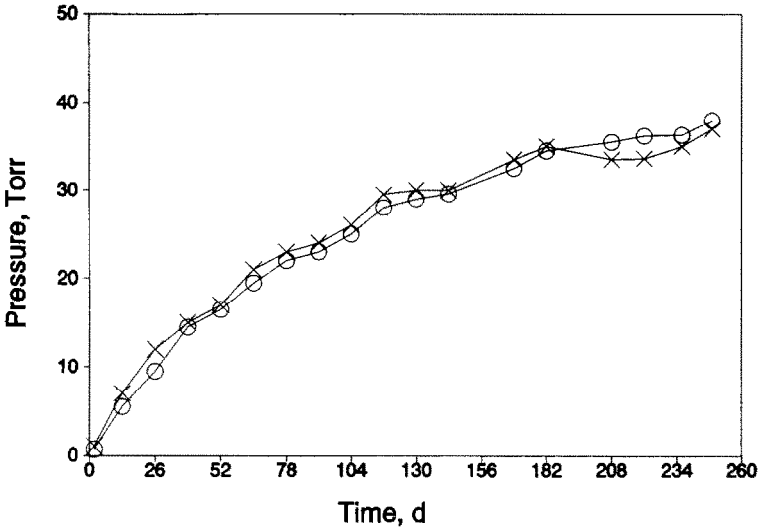

Fig. 5. Observed and calculated NO evolution profiles at 383 K: ×, obs. NO; ○, calc. NO for 5500 $cm^2 g^{-1}$ PETN.

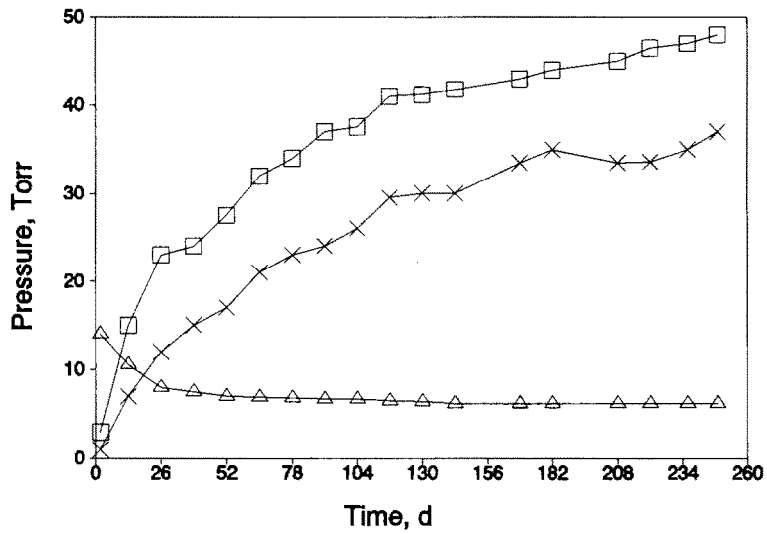

Fig. 6. Predicted NO and NO_2 evolution profiles at 383 K under an initial pressure of 15 torr of NO_2: ×, obs. NO for 5500 $cm^2 g^{-1}$ PETN under vacuum; □, calc. NO for $P^0_{NO_2} = 15$ torr; △, Calc. NO_2 for $P^0_{NO_2} = 15$ torr.

DISCUSSION

Figures 1 and 2 reveal that TMR is correlated to surface area; TMR increases with the surface area. The breadth of the temperature range for the data given in Fig. 2 prohibits a totally quantitative analysis; however, three points are significant. Firstly, the apparent slopes for the data suggest

that each sample reacts with different A and E parameters; variations of activation parameters with surface area are contrary to expectations that decomposition occurs homogeneously, with E equivalent to the O–NO_2 bond fission enthalpy [1, 3]. The 5000 $cm^2 g^{-1}$ PETN is the only sample that indicates activation parameters consistent with homogeneous bond fission. Secondly, at the high end of the temperature range, the data suggest coalescence to a common point; this indicates that reactivity may be independent of initial surface area at high temperature. Thirdly, the magnitudes of the slopes given in Fig. 2 indicate that the stability order with respect to surface area is $5000 < 5500 < 12\,000\ cm^2 g^{-1}$.

It is known that thermal aging changes the surface area of PETN. This observation suggests that reactivity is governed by changes in surface area and perturbations arising from stabilizers and residual solvents. Thermal aging would minimize the surface free energy, decrease the surface area, and increase the mean particle size of PETN. Free energy minimization would be dominated by an increase in lattice entropy and increase the number of sites within the lattice available for decomposition. This mechanism is in accord with the reactivity–particle-size correlation of Myers [15], and the crystal habit study of Rogers and Dinegar [16].

Profiles for NO evolution from PETN at 383 K given in Fig. 3 imply a stability order consistent with the TMR data discussed above. These observations agree with the conclusion of Myers [15] related to gas evolution from single crystals of PETN at 393 K: reaction rates for single crystals are directly proportional to particle size; particle size is inversely proportional to surface area. However, these observations are contrary to the trend given in Fig. 4 at 363 K which suggests that stability decreases with increasing surface area. The data of Fig. 4 are in accord with NO_2 evolution determined at 323 K by Volltrauer [17] which indicates enhanced reactivity with higher surface area. Below 383 K, thermal microscopy [16] indicates that aging of high surface area PETN may produce additional crystal imperfections as the mean particle size increases and the surface area decreases. This phenomenon would lead to additional surface-active sites; therefore, the apparent dichotomy between the TMR data and the NO evolution observed at 363 K could be altered at lower temperatures.

Figure 5 reveals that agreement between the observed and calculated NO evolution at 383 K is reasonable. The explicit assumption that initiation is primarily in the solid state is consistent with the absence of an endotherm [3] in the thermograms depicted in Fig. 1 and the fact that gas phase initiation governed by sublimation (reaction (1, −1)) is too small to account for the observed pressure change associated with decomposition below the normal melting point. Reactions (8) and (9)

(8) $C(CH_2ONO_2)_4 + NO_2 \rightarrow C(CH_2ONO_2)_3CHONO_2 + HNO_2$

(9) $C(CH_2ONO_2)_3CHONO_2 \rightarrow C(CH_2ONO_2)_3 + CO + HNO_2$

were proposed as a potential mechanism for gas-phase autocatalysis in the decomposition of PETN. The importance of these reactions is also limited by the sublimation pressure of PETN; however, they would be significant in the liquid phase at temperatures above the melting point.

Inclusion of the equilibrium represented by reaction (11, −11) was necessary in order to ensure that the NO reaction rate decreased at times exceeding 100 days

(11, −11) $2NHO_2 \rightleftharpoons H_2O + NO + NO_2$

Reactions (11, −11) were used by Lin et al. [5] in kinetic modeling for the chain reaction of H_2CO and NO_2 (reaction (20) in Appendix A). The sensitivity analysis performed by varying the activation energies for selected reactions revealed that the calculated NO profile was strongly influenced by reactions (2), (5), (6), (11, −11), and (20).

The NO evolution profile calculated numerically for PETN under an initial pressure of 15 torr of NO_2 given in Fig. 6 indicates that NO_2 accelerates the production of NO. Elimination of $k_{11}[HNO_2]^2$ from the series of reactions given in Appendix A by application of the steady state assumption for $[NHO_2]$ and neglect of reaction (46) leads to eqns. (4) and (5)

$$\frac{d[NO]}{dt} \approx I_1 + \{k_8[C(CH_2ONO_2)_4] + k_{10}[CH_3O] + k_{16}[CHO] + k_{17}[H] + k_{20}[H_2CO] + k_{21}[CH_3ONO_2] + k_{28}[CO]\}[NO_2] - \{k_{14}[CHO] + k_{27}[CH_3O] + k_{29}[N_2O] + k_{33}[O_2] + 2k_{34}[NO][O_2] + k_{38}[H][M]\}[NO] \quad (4)$$

$$\frac{d[NO_2]}{dt} \approx I_2 + \{k_{30}[OH] + k_{33}[O_2] + 2k_{34}[O_2][NO]\}[NO] - \{(k_2 + k_3)[C(CH_2ONO_2)_3CH_2O] + k_7[CH_3O] + k_{12}[H_2O] + k_{16}[CHO] + k_{17}[H] + k_{28}[CO]\}[NO_2] \quad (5)$$

where

$$I_1 = (k_5 + k_6)[C(CH_2ONO_2)_3] + k_9[C(CH_2ONO_2)_3CHONO_2] + k_{26}[CH_3ONO] + k_{-30}[NHO_2][M] + k_{39}[NHO][O] + k_{40}[NHO][H] + k_{42}[CHO][HNO] - k_{44}[NHO_2][OH] - k_{45}[NHO_2][H]$$

and

$$I_2 = k_2[C(CH_2ONO_2)_4(c)] + k_3[C(CH_2ONO_2)_4] + k_7[CH_3ONO_2] + k_9[C(CH_2ONO_2)_3CHONO_2] + k_{22}[CH_2ONO_2] + k_{41}[HNO][O]$$

Equations (4) and (5) indicate that the relative rates of NO and NO_2 production will be determined by the relative concentrations of NO, NO_2, and O_2. Equation (4) predicts that addition of NO_2 will accelerate and decelerate NO production in the early and latter stages of reaction, respectively. In eqn. (5) the rate of change of NO_2 will be dominated by reactions (16), (17), and (34) and the relative concentrations of O_2 and NO_2. Under conditions where O_2 pressure is high, e.g., an air atmosphere, eqn. (5) indicates that NO_2 will exhibit a maximum due to the oxidation of NO in reaction (34). When O_2 pressure is low or if NO_2 is present initially, the rate will be dominated by reactions such as (16) and (17) involving H and CHO radicals. The analysis is consistent with the numerical calculations illustrated in Fig. 6.

Predictions based on eqns. (4) and (5) and the numerical calculations in Fig. 6 have been recently confirmed by Dosser [19], who monitored depletion of NO_2 at 550 nm. Preliminary data for 12 000 $cm^2\,g^{-1}$ PETN under an initial pressure of 40 torr of NO_2 illustrated in Fig. 7 confirms that the addition of NO_2 accelerates the production of NO. The qualitative consistency between the predictions of eqns. (4) and (5) and the experimental data given in Fig. 7 adds credibility to the detailed

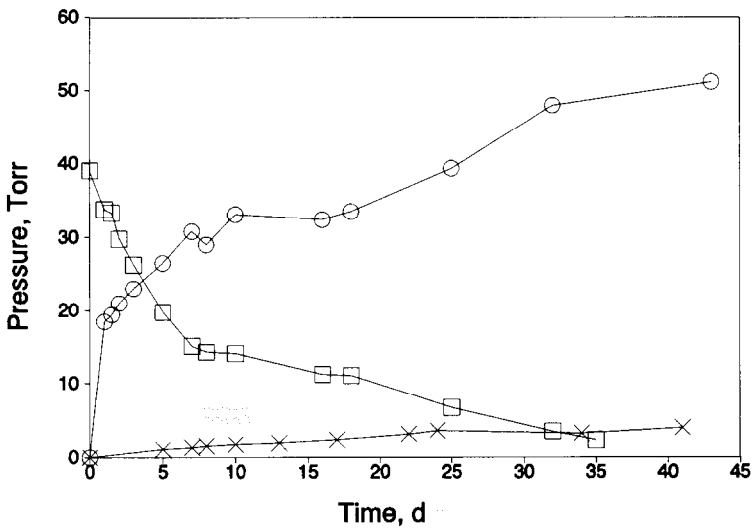

Fig. 7. Observed acceleration of NO evolution with added NO_2 at 363 K: ○, obs. NO for 12 000 $cm^2\,g^{-1}$ PETN with $P^0_{NO_2} = 40$ torr; ×, obs. NO evolution for 12 000 $cm^2\,g^{-1}$ PETN under vacuum; □, obs. depletion of NO_2 for $P^0_{NO_2} = 40$ torr.

mechanism used in the kinetic modeling. The kinetic model also provides a quantitative explanation for the fact that TMR is reduced when NO_2 and/or O_2 are present in the atmosphere. Here, secondary reactions arising from chain transfer and initiation by NO_2 (reactions (10), (16), (17), (20), and (21)), or oxidation of NO by O_2 (reaction (34)) reduce the magnitude of the differential $f(\alpha)^{-1}\,d\alpha$ which leads to a smaller TMR.

REFERENCES

1 J.M. Pickard, Solid-state decomposition kinetics of pentaerythritol tetranitrate, Proc. 19th NATAS Conference, Boston, MA, 23–26 September 1990, pp. 346–351.
2 K. Ebert, H. Ederer and T.L. Isenhour, Computer Applications in Chemistry, VCH, New York, 1989, pp. 510–522.
3 W.L. Ng, J.E. Field and H.M. Hauser, J. Chem. Soc. Perkin Trans. 2, (1976) 637.
4 R.H. Dinegar and M. Stammler, Explosivstoffe Nr., 1 (1971) 14.
5 Y. He, E. Kolby, P. Shumaker and M.C. Lin, Int. J. Chem. Kinet., 21 (1989) 1015.
6 C.Y. LIn, H.T. Wang, M.C. Lin and C.F. Melius, Int. J. Chem. Kinet., 22 (1990) 455.
7 P. Gray, J.F. Griffiths and K. Hasegawa, Int. J. Chem. Kinet., 13 (1981) 817.
8 L. Batt, R.D. McCulloch and R.T. Milne, Int. J. Chem. Kinet., 6 (1974) 945.
9 G. Baker and R. Shaw, J. Chem. Soc., (1965) 6965.
10 G. Dixon-Lewis, M.M. Sutton and A. Williams, J. Chem. Soc., (1965) 5724.
11 R.G. Jungst (Ed.), C-4 Trident Missile Body Ordinance Aging GAMS Program Biannual Report for March to October 1981, Sandia Report SAND82-0707, April 1982, p. 19.
12 T.R. Gibbs and A. Popolato (Eds.), LASL Explosive Property Data, University of California Press, Berkeley, 1980, p. 134.
13 A.F. Trotman-Dickenson and G.S. Milne, Tables of Bimolecular Gas Reactions, NSRDS-NBS9, 1967.
14 S.W. Benson, Thermochemical Kinetics, John Wiley, New York, 2nd edn., 1976, pp. 108–117.
15 L.C. Myers, Quarterly Progress Report, Lawrence Livermore National Laboratory, October 1974.
16 R.N. Rogers and R.H. Dinegar, Thermochim. Acta, 3 (1972) 367.
17 H.N. Volltrauer, Thermochim. Acta, 5 (1982) 353.
18 C.M. Love, EG&G Mound Applied Technologies, Miamisburg, OH, personal communication, 12 October 1992.
19 L.R. Dosser, EG&G Mound Applied Technologies, Miamisburg, OH, unpublished data.

APPENDIX A: REACTIONS FOR KINETIC MODELING OF PETN DECOMPOSITION

Number	Reaction
1, −1	$C(CH_2ONO_2)_4(c) \rightleftharpoons C(CH_2ONO_2)_4$
2, −2	$C(CH_2ONO_2)_4(c) \rightleftharpoons C(CH_2ONO_2)_3CH_2O + NO_2$
3, −3	$C(CH_2ONO_2)_4 \rightleftharpoons C(CH_2ONO_2)_3CH_2O + NO_2$
4	$C(CH_2ONO_2)_3CH_2O \rightarrow C(CH_2ONO_2)_3 + H_2CO$
5	$C(CH_2ONO_2)_3 \rightarrow 2CH_2ONO_2 + 2CO + NO$

APPENDIX A (*continued*)

Number	Reaction
6	$C(CH_2ONO_2)_3 \rightarrow 2CH_2ONO_2 + NO + H_2CO + CO$
7, −7	$CH_3ONO_2 \rightleftharpoons CH_3O + NO_2$
8	$C(CH_2ONO_2)_4 + NO_2 \rightarrow C(CH_2ONO_2)_3CHONO_2 + HNO_2$
9	$C(CH_2ONO_2)_3CHONO_2 \rightarrow C(CH_2ONO_2)_3 + CO + HNO_2$
10	$CH_3O + NO_2 \rightarrow H_2CO + HNO_2$
11, −11	$2HNO_2 \rightleftharpoons H_2O + NO + NO_2$
12	$NO_2 + H_2O \rightarrow HNO_2 + OH$
13	$CH_3O + H_2CO \rightarrow CH_3OH + CHO$
14	$CHO + NO \rightarrow CO + NHO$
15	$2HNO \rightarrow H_2O + N_2O$
16	$CHO + NO_2 \rightarrow H + CO_2 + NO$
17	$H + NO_2 \rightarrow OH + NO$
18	$H + H_2CO \rightarrow CHO + H_2$
19	$OH + H_2CO \rightarrow CHO + H_2O$
20	$H_2CO + NO_2 \rightarrow CHO + HNO_2$
21	$CH_3ONO_2 + NO_2 \rightarrow CH_2ONO_2 + HNO_2$
22	$CH_2ONO_2 \rightarrow H_2CO + NO_2$
23	$H_2CO + CH_2ONO_2 \rightarrow CH_3ONO_2 + CHO$
24	$CHO + CH_2ONO_2 \rightarrow CH_3ONO_2 + CO$
25	$OH + CO \rightarrow H + CO_2$
26, −26	$CH_3ONO \rightleftharpoons CH_3O + NO$
27	$CH_2O + NO \rightarrow H_2CO + HNO$
28	$NO_2 + CO \rightarrow NO + CO_2$
29	$NO + N_2O \rightarrow NO_2 + N_2$
30, −30 [a]	$OH + NO + M \rightleftharpoons HNO_2 + M$
31	$H + N_2O \rightarrow OH + N_2$
32	$HNO + OH \rightarrow H_2O + NO$
33	$O_2 + NO \rightarrow O + NO_2$
34	$2NO + O_2 \rightarrow 2NO_2$
35	$CO + O_2 \rightarrow CO_2 + O$
36 [a]	$CO + O + M \rightarrow CO_2 + M$
37	$CHO + OH \rightarrow H_2O + CO$
38 [a]	$NO + H + M \rightarrow HNO + M$
39	$HNO + O \rightarrow NO + OH$
40	$HNO + H \rightarrow H_2 + NO$
41	$HNO + O \rightarrow NO_2 + H$
42	$CHO + HNO \rightarrow H_2CO + NO$
43 [a]	$2O + M \rightarrow O_2 + M$
44	$HNO_2 + OH \rightarrow NO_2 + H_2O$
45	$HNO_2 + H \rightarrow NO_2 + H_2$
46	$NO + HNO_2 \rightarrow NO_2 + HNO$
47	$OH + O \rightarrow H + O_2$
48	$OH + H_2 \rightarrow H_2O + H$
49	$2OH \rightarrow H_2O + O$

[a] In reactions (30), (36), (38), and (43), the concentration of the third body was fixed at [M] = 0.03184.

APPENDIX B: RATE PARAMETERS FOR PETN DECOMPOSITION REACTIONS [a]

Reaction number	log A	n	E	Ref.
1	14.0	0.0	146.3	4
−1	−0.84	0.0	−0.3	[b]
2	14.3	0.0	160.9	11
−2	9.6	0.0	0.0	[b]
3	16.5	0.0	165.1	1, 3
−3	9.6	0.0	0.0	[b]
4	15.0	0.0	20.9	[c]
5	13.0	0.0	108.6	[c]
6	13.0	0.0	100.3	[c]
7	14.5	0.0	163.8	7
−7	9.6	0.0	0.0	[b]
8	9.2	0.0	96.1	[c]
9	13.0	0.0	41.8	[c]
10	8.6	0.0	0.0	[d]
11	8.8	0.0	34.7	5
−11	3.23	0.0	0.0	5
12	10.3	0.0	185.5	[c]
13	8.3	0.0	0.0	[c]
14	10.84	−0.4	0.0	5
15	5.92	0.0	16.3	5
16	9.93	0.0	0.0	5
17	11.4	0.0	3.4	5
18	6.47	1.27	11.0	5
19	10.0	0.0	0.7	5
20	8.46	0.0	53.7	6
21	9.2	0.0	108.7	[c]
22	11.0	0.0	8.2	[c]
23	9.0	0.0	0.0	[c]
24	11.0	0.0	0.0	[c]
25	4.17	1.3	−3.2	5
26	15.8	0.0	172.2	8
−26	10.3	0.0	0.0	[b]
27	9.6	0.0	0.0	8
28	9.1	0.0	115.3	6
29	11.4	0.0	209.0	13
30	11.2	−0.5	0.0	6
−30	15.6	0.0	206.1	[b]
31	10.7	0.0	54.3	10
32	9.1	0.5	8.3	6
33	4.86	1.49	190.6	6 [b]
34	6.42	0.0	−1.67	6 [b]
35	10.2	0.0	171.4	6
36	11.8	0.0	12.5	6
37	10.5	0.0	0.0	6
38	9.73	0.0	−2.5	6
39	5.69	0.5	8.31	6
40	10.11	0.0	16.6	6

APPENDIX B (*continued*)

Reaction number	log A	n	E	Ref.
41	7.69	0.5	8.4	6
42	9.3	0.0	20.9	6
43	7.27	0.0	7.5	6
44	10.0	0.0	12.5	6
45	9.0	0.0	4.18	6
46	11.0	0.0	118.7	[c]
47	11.56	−0.5	0.0	6
48	10.72	0.0	27.2	6
49	5.77	1.3	0.0	6

[a] Rate constants are expressed as $k = AT^n 10^{-E/\theta}$ where $\theta = 2.303RT$ kJ mol^{-1}. Units of A for second- and third-order reactions are dm^3 mol^{-1} s^{-1} and dm^6 mol^{-2} s^{-1}, respectively. [b] Estimated from reverse reaction thermochemistry using $\log(A_i/A_{-i}) = (\Delta S^{\ominus}_{i,-i} - \Delta nR(1 + \ln(R'T))/(2.303R)$ and $E_{-i} = E_i - \Delta H^{\ominus}_{i,-i} - \Delta nRt$. Units for R and R' are J K^{-1} mol^{-1} and dm^3 atm K^{-1} mol^{-1}, respectively. [c] Estimated from group additivity. [d] Estimated from $k_7/k_{10} = 2.7$ from ref 9.